Available online at www.sciencedirect.com
SCIENCE DIRECT
Polymer 46 (2005) 12065–12072
polymer
www.elsevier.com/locate/polymer

Thermo-mechanical characterization of fumed silica-epoxy nanocomposites

Michele Preghenella *, Alessandro Pegoretti, Claudio Migliaresi

Department of Materials Engineering and Industrial Technologies and INSTM Research Unit, University of Trento, via Mesiano, 77, 38050 Trento, Italy

Received 5 August 2005; received in revised form 11 October 2005; accepted 20 October 2005
Available online 10 November 2005

Abstract

DGEBA-based epoxy nanocomposites filled with various amounts of fumed silica nanopowders (10, 20 and 30 phr corresponding to 3.3, 6.4 and 9.2% by volume) were prepared by a solvent assisted dispersion procedure. The obtained nanocomposites were analyzed by means of differential scanning calorimetry, dynamic-mechanical thermal analysis, uniaxial tensile tests on un-notched samples and three-point bending tests on notched samples.

All the thermal and mechanical properties showed non-monotonic trends with relative minima as the silica content increased. A trend inversion in the physical properties was detected at the highest filler level tested, which was not previously observed for epoxy systems filled with comparable amounts of unmodified silica. The behavior could be explained by considering a reduction of cross-linking degree of the epoxy matrix due to the huge viscosity increase induced by the silica nanoparticles during composites preparation. On the other hand, the physical immobilization of the cross-linked matrix can be supposed to be responsible for the inversion of the properties trend at the highest filler level, which is presumably very close to the percolation threshold.

Keywords: Epoxy-silica nanocomposites; Thermal properties; Mechanical properties

1. Introduction

Nanocomposites are a class of composite materials in which the dimensions of the dispersed phase are nanometric. In some cases, nanocomposites exhibit greatly improved properties with respect to conventional microcomposites loaded with the same amount of reinforcing phase, thus allowing for a potential weight-saving design of many plastic products.

At least three class of nanocomposites can be distinguished, depending on the morphology of the filler: layered nanocomposites, whisker (or nanotubes) based nanocomposites and isodimensional nanocomposites. In recent years, the attention has been mainly focused on the first class of nanocomposites, especially those obtained from layered silicates [1,2] in thermoplastic or thermosetting matrices [3] since they often demonstrated a remarkable improvement in thermal and mechanical properties with respect to traditional microcomposites. Other fillers, such as carbon black or fumed silica, have been largely used as additives to improve the properties of polymers, for example to impart uv-resistance or to control rheological properties, and quite recently, were also considered as nanometric fillers with potentially interesting reinforcing capabilities.

Unfortunately, they did not always fulfill the expectations depending on the particular polymeric matrix in which they were used and the specific surface treatment. For instance silica nanoparticles were found to decrease the glass transition temperature in LLDPE matrix-based nanocomposites [4]. A reduction of T_g has been also previously reported for thermoplastic polyurethane-fumed silica composites [5] as the surface area of the filler exceeded 200 m^2/g. On the contrary, DMTA tests evidenced a secondary relaxation signal, at a temperature 40 °C higher than T_g, ascribed to the presence of an immobilized matrix layer near the filler surface in silica-filled styrene-butadiene block copolymers [6]. Similarly, in PVAc, P4VP, PMMA and PS the addition of silica nanoparticles induced the development of two distinct glass transitions observed in DMTA tests [7,8] the higher T_g being attributed to the formation of an immobilized polymeric phase around the filler.

More recently, Sun and co-workers [9] compared the effects of nano-sized and micro-sized fillers in epoxy composites by means of differential scanning calorimetry, thermo-mechanical and dielectric relaxation measurements thus evidencing that the glass transition temperature was reduced as the nanofiller amount increased whereas it did not change in the

* Corresponding author. Tel.: +39 461 882411; fax: +39 461 881977.
E-mail address: michele.preghenella@ing.unitn.it (M. Preghenella).

0032-3861/$ - see front matter © 2005 Elsevier Ltd. All rights reserved.
doi:10.1016/j.polymer.2005.10.098

corresponding microcomposites. Contrasting effects have also been reported in other works for different fillers in various matrices: both an increase [10] and a decrease [11] of the thermo-mechanical properties were reported and sometimes even more complicated non-monotonic trends were observed with the best performance at filler level as low as 5% by weight [12].

From this literature survey it is clear that the performance of different nanocomposites systems is difficult to compare and the same filler may produce different effects in different matrices or even in the same matrix under different processing conditions. The need to improve the mechanical properties of epoxy matrices is encouraging the use of silica nanoparticles as reinforcing agent: till now, the best performance was obtained with surface functionalized nanoparticles [13]. On the other hand, untreated silica nanoparticles appeared to deteriorate thermal properties in epoxy matrices mainly because of the presence of residual moisture and organics [14]. The aim of this work is to study the effects of untreated silica nanopowders in an epoxy matrix and to investigate the interactions occurring between filler and matrix with thermal analysis, DMTA and mechanical tests. In order to avoid spurious effects we decided to use high surface area pirogenic silica, rather than sol–gel silica, since it is free from organic residua, being obtained by a flame process at 1800 °C. Moreover we also adopted a solvent assisted preparation procedure in order to promote matrix–filler interactions and prevent moisture contamination during the preparation of the composite blends.

2. Experimental section

2.1. Materials

The selected epoxy matrix was a commercial bicomponent system (EC57/K63), supplied by Camattini. (Collecchio, Parma, Italy), consisting of a DGEBA-based low molecular weight epoxy resin (EC57: epoxy-equivalent 172–182 g/equiv) and a polyamide-amine curing agent (K63: 88–91 g/equiv). The filler was the Cab-O-Sil M5 fumed silica, supplied by Cabot GmbH (Hanau, Germany), consisting of aggregates of untreated pure amorphous silica nanoparticles, with nominal surface area of about 200 m^2/g.

2.2. Composites preparation

Composite samples were prepared with filler loadings of 10, 20 and 30 phr (corresponding to 6.3, 11.8 and 16.7% by weight and to 3.3, 6.4 and 9.2% by volume, respectively) according to the following procedure. Both the epoxy resin and the hardener were degassed in vacuum at 80 °C for 6 h. The necessary amount of resin EC57 and silica particles were mixed and diluted with 200 phr of acetone (Sigma-Aldrich A4206, ACS reagent minimum 99.5%) in a flask kept in a water bath at 70 °C. The solution was vigorously stirred by the boiling solvent while its vapors were recovered and condensed with a distillation column for 30 min. The acetone content in the solution was then reduced to 100 phr and the mixture was cooled down to room temperature. The 50 phr nominal stoichiometric amount of hardener K63 was hence added and dispersed by sonication for 30 min in a Branson 2510 ultrasonic bath (47 kHz, 125 W). The composite paste was poured in a two-halves square Teflon® mould (cavity dimensions: 100 mm × 100 mm × 2 mm) confined between two stainless steel plates. The mixture was degassed at 0.05 atm for 30 min placing the open mould in a plexiglass® vacuum-chamber mounted on a shaking table. After degassing the moulds halves were closed, loaded in a press with a compressive force of 1 ton and screwed to keep the specimens under compression during the curing stages. All samples were hold for 24 h at 25 °C and for 15 h at 60 °C, then the mould was opened and the samples were punch-cut from the obtained sheets according to the 1BA dumb-bell geometry described in the ISO 527/2(97) standard. Finally, the dumb-bells were post-cured in an oven at 120 °C and 0.2 atm for 6 h. The same procedure was also adopted for the preparation of unfilled epoxy resin sample used as reference material.

All the samples were kept in sealed vacuum bags stored at −80 °C to prevent moisture pick-up and aging of the epoxy matrix.

2.3. Testing procedures

Differential scanning calorimetry (DSC) analysis was performed with a Mettler DSC 30 calorimeter at an heating rate of 10 °C/min in the temperature range from −50 up to 230 °C in nitrogen flux (200 ml/min) with samples loaded in 40 μl aluminum pans provided with venting holes. According to ASTM D3418 standard, the sample mass was in the range 10–20 mg and the glass transition temperature (T_g) was assessed by the mid-point construction. For each specimen three consecutive scans were performed under the same conditions.

Thermogravimetric (TGA) analysis was performed by a Mettler TG50 thermogravimetric balance connected to a Mettler TC10A processor. The scans were performed at 10 °C/min in nitrogen atmosphere (200 ml/min) in the temperature range from 30 up to 300 °C.

The initial moisture content in the samples was determined by TGA analysis as the difference in the weight loss between the material under investigation and the reference matrix dried up to 230 °C.

Water sorption tests were performed on the epoxy matrix in order to quantify the effects of moisture residua on the glass transition temperature. Small samples of 10–15 mg were exposed to water vapor in a flask at 75 °C. The samples were not directly immersed in water and the vapor pressure was kept below the saturation limit by adding $CaCl_2$ to water in order to obtain a solution with a mole fraction of dissolved salt equal to 0.1. At scheduled times the water up-take was measured by TGA analysis assessing the weight loss of the samples with respect to a dry reference sample separately prepared by vacuum drying the cured epoxy at 75 °C and 0.02 atm for 10 h. DSC analysis was used to determine the glass transition

temperature depression of the epoxy matrix caused by the absorbed humidity.

Mechanical tests were performed both in uniaxial tensile and three-point bending configurations using an Instron 4502 testing machine. Samples for tensile tests conformed to UNI EN ISO 527 type 1BA dumb-bell geometry. Tensile tests were performed at a strain rate of 0.01 min^{-1} and an electric extensometer was used to asses the tensile modulus. Samples for three-point bending tests were machined from the central part of untested dumb-bell pieces to obtain single-edge notched samples (SENB) conforming to ASTM D5045 standard test method for plane-strain fracture toughness and strain energy release rate of plastic materials. Samples were tested to failure at a cross-head speed of 1 mm/min. Fractured surfaces were observed with a SEM microscope JEOL JSM 5500 at magnifications from 35× up to 20,000×. According to ASTM D4065 standard, the samples for dynamic-mechanical tests were bars of rectangular section, 30 mm long, 5 mm wide and 2 mm thick. All the specimens were carefully polished and visually inspected for flaws. Dynamic mechanical thermal analysis measurements were performed using a MkII Polymer Laboratories DMTA testing-machine (Loughborough, UK). Tests were performed in tensile mode, applying a static stress of 0.5 MPa and a peak-to-peak displacement of 32 μm. Single-frequency tests at 1 Hz were performed at a constant heating rate of 3 °C/min, in the temperature range from −50 up to 200 °C. Multi-frequency tests were performed at a constant heating rate of 0.5 °C/min in the temperature range from −100 up to 150 °C at the frequencies of 0.3, 1, 3, 5, 10 and 30 Hz.

3. Results and discussion

As clearly shown in Fig. 1, DSC analysis performed on the cured composites evidenced a reduction in their glass transition temperature with respect to the unfilled matrix. The effect was non-monotonic with the filler amount and, at a silica content of 30 phr, the trend of T_g values showed an inversion. This behavior was observed in both the first and the second DSC scans. It is worth noting that a rise in the T_g's values occurred between first and second DSC scans. At the same time, a small weight loss was detected for the composites and the unfilled matrix at the end of the first DSC scan which was due to the evolution of volatile products (see Table 1). This weight loss was also confirmed by the data obtained by thermogravimetric analysis in the same temperature range and reported in Table 1. On the other hand, no substantial weight losses nor variations in T_g's values were detected in successive DSC scans (see Fig. 1). Sun and co-workers also noticed a reduction in the glass transition temperatures of silica filled epoxies [9] that they ascribed to the presence of residual moisture and organics on the surface of sol–gel silica-nanoparticles they used. The presence of residual organics on silica surface was excluded in our case because we employed fumed-silica nanoparticles produced by a flame process at 1800 °C. TGA analysis on these particles evidenced an average weight loss of about 2% up to 230 °C due to release of moisture and the same weight loss is reported on the product data sheet up to 1000 °C. The presence of moisture in high-surface area silica nanoparticles is very difficult to avoid since immediately after drying the powders rapidly re-adsorb the equilibrium humidity content within few minutes of exposure to air at laboratory conditions (25 °C and 50% RH). Since water-residua are well known to play an important role in lowering the glass transition temperature of epoxies [15] we performed water-uptake experiments on the unfilled matrix to asses the T_g depression due to water uptake. The results, reported in Fig. 2, clearly demonstrated that a substantial T_g depression was observed as a function of

Table 1
Weight losses

Silica content (phr)	Weight loss after DSC (up to 230 °C) I scan (%)	Weight loss after TGA (up to 230 °C) (%)	Estimated moisture due to silica[a] (%)
Dry sample	1.5±0.4	1.3±0.3	–
0	1.4±0.4	1.6±0.3	–
10	1.6±0.3	1.3±0.3	0.13
20	2.0±0.4	1.9±0.5	0.27
30	2.5±0.3	2.2±0.5	0.40

The weight losses are normalized to the polymer content.
[a] The value is calculated for 2% by weight of moisture in silica nanoparticles as measured by TGA up to 250 °C.

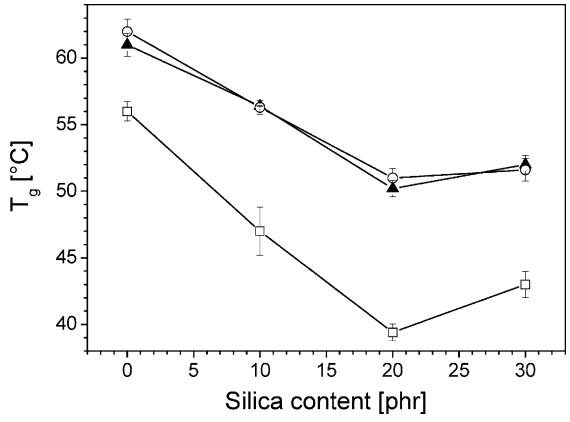

Fig. 1. Glass transition temperature measured by DSC analysis. First scan (□), second scan (▲), third scan (○).

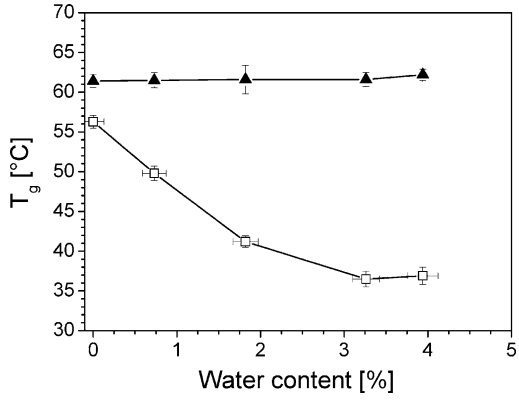

Fig. 2. Effect of moisture residua on glass transition temperature of the epoxy matrix. First scan (□), second scan (▲).

the absorbed water and that the water was completely removed at the end of the first DSC scan. In fact, the T_g values obtained in the second DSC scan remained practically unperturbed with respect to the dry reference sample. By comparing the weight losses of dry and unfilled polymer matrix with those of the composites (Table 1) we expected that the moisture present on silica nanopowders was removed during the first DSC scan. Moreover, from these data and those presented in Fig. 2, the maximum glass transition depression expected for the moisture content of the silica particles should be less than 3–4 °C. Since we observed a much more consistent T_g depression in the first scan on composites and the same trend was found during successive scans, we supposed that water moisture was not the only factor determining the observed trends. We postulated that silica-nanoparticles actually induced a reduction in the cross-linking degree of the polymer matrix by effectively preventing the complete curing of the epoxy up to temperatures as high as the onset-temperature of polymer degradation. Moreover, an inversion in the trend of thermal properties occurred at 30 phr filler level, which could be explained by the occurrence of better physical immobilization of polymer chains near the filler surface at the highest filler level, that we suppose to be close to the percolation threshold.

Since the minimum amount of filler examined in this work is 10 phr, that corresponds to 6.3% by weight and 3.3% by volume, we cannot exclude that different effects could be observed at lower filler content, as already observed in other polymeric matrices [10,12].

Mechanical tests were performed to quantify the overall effect of the filler on the performance of the composites. Tensile stress–strain curves are shown in Fig. 3 and the resulting properties are reported in Table 2. At filler loadings of 10 and 20 phr the silica-nanoparticles markedly plasticized the epoxy matrix reducing its elastic modulus, yield stress and tensile strength, while noticeably increasing its strain at break. Only for the 30 phr filled sample an increase of tensile modulus was observed, even if the yield stress and the ultimate tensile strength did not improve with respect to the unfilled matrix. These results are in agreement with the postulated reduction in cross-linking degree of the matrix and with the possible occurrence of better physical interactions between polymer phase and filler at the highest silica loading tested.

Table 2
Tensile properties

Silica content (phr)	Elastic modulus E (MPa)	Stress (MPa)		Strain (%)	
		At yield	At break	At yield	At break
0	2260±71	35.3±0.8	30.2±0.9	3.8±0.1	12.0±1.7
10	1500±120	17.8±0.8	19.7±0.3	4.1±0.1	27.2±0.5
20	1900±150	21.3±0.6	23.8±1.0	3.8±0.4	26.0±2.1
30	2800±240	25.0±0.6	24.9±0.7	4.0±1.2	8.0±2.9

Three point bending tests have been performed on SENB specimens in order to assess the fracture toughness of the nanocomposites. Both the critical values of the stress intensity factor and strain energy release rate were assessed as apparent values (K_{IQ} and G_{IQ}) because the radius of the plastic zone at the notch-tip was found to exceed the limit established by ASTM D5045 standard for the application of linear elastic fracture mechanic (LEFM). The values of G_{IQ} and K_{IQ} are reported in Fig. 4. It is interesting to observe that at low silica content (10 phr) the fracture toughness of the composite exceeded that one of the unfilled polymer matrix and then it decreased again as the silica content increased.

In Fig. 5 the SEM images of the fracture surfaces of nanocomposites and unfilled epoxy matrix are compared at low magnification (35×). It is worth noting that the crack propagation was accompanied by a quite large plastic deformation over the whole ligament section in 10 and 20 phr filled samples. On the contrary the behavior of 30 phr filled samples was comparatively much more brittle and similar to that observed for the unfilled matrix with limited plastic deformation confined in the region just ahead the notch-tip. At higher magnification (20,000×) the fracture surface of the unfilled matrix appeared very smooth, whereas the composites samples showed a much more rough pattern with sub-micrometric clusters of particles emerging from their surface (see Fig. 6). It was observed that the relative amount of aggregates is higher in the 20 phr filled samples but surprisingly it appeared to be remarkably reduced at 30 phr.

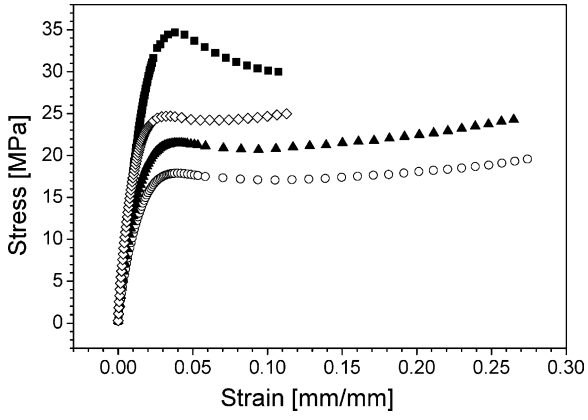

Fig. 3. Stress–strain curves as determined in uniaxial tension for silica content of 0 phr (■), 10 phr (○), 20 phr (▲), 30 phr (◇).

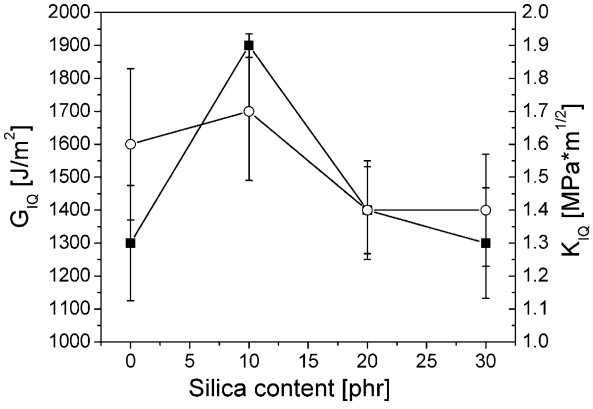

Fig. 4. Apparent critical energy release rate G_{IQ} (■) and apparent fracture toughness K_{IQ} (○) measured in three-point bending test on notched specimens.

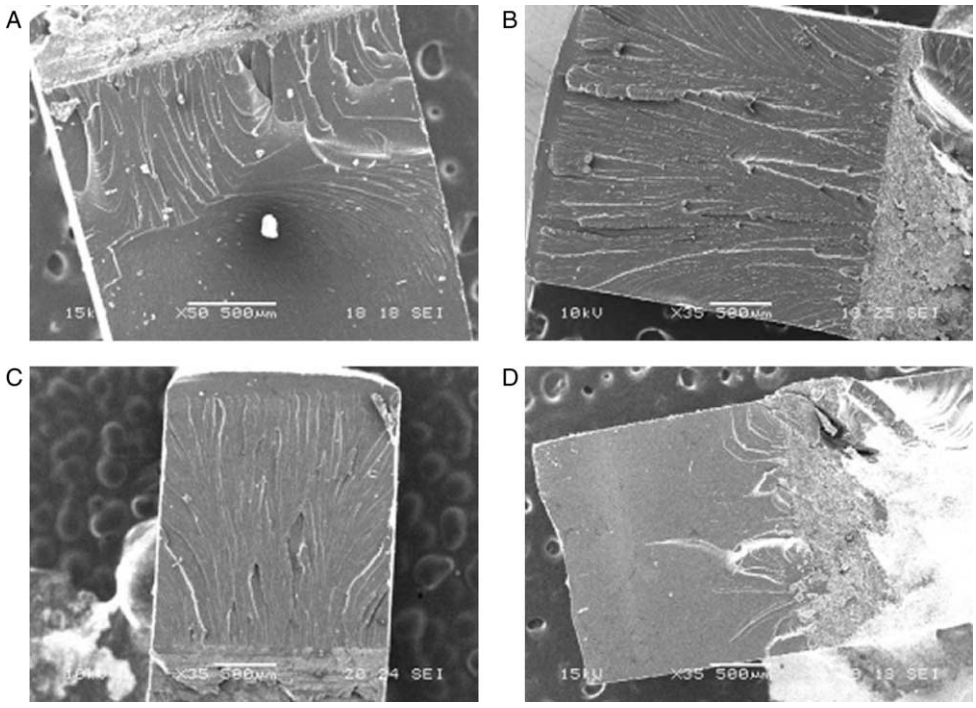

Fig. 5. Low magnification (35×) SEM images of fracture surfaces of nanocomposites obtained in three-point bending set up: unfilled matrix (A), 10 phr silica filled sample (B), 20 phr (C) and 30 phr (D). The dimension of the marker is 500 μm in all the micrographs.

This trend could be explained by supposing an improvement of the filler–matrix interactions for 30 phr filled samples, and therefore a crack propagation path occurring inside the epoxy matrix. Further investigations have been performed by means of atomic force acoustic microscopy (AFaM) [16] in order to statistically quantify the distribution of the filler by measuring the local elastic stiffness of the fracture surface. The results obtained confirmed a reduction in the exposure probability of

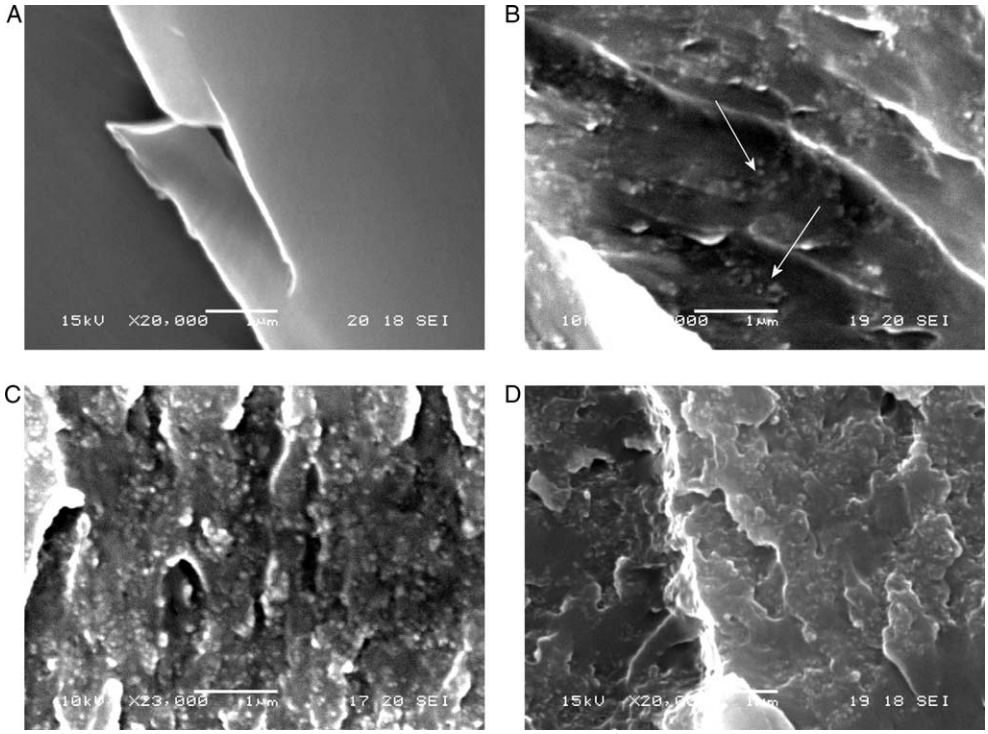

Fig. 6. High magnification (20,000×) SEM images of fracture surfaces of nanocomposites obtained in three-point bending set up: unfilled matrix (A), 10 phr silica filled sample (B), 20 phr (C) and 30 phr (D). The dimension of the marker is 1 μm in all the micrographs. Arrows in (B) point to silica particles exposed on the surface.

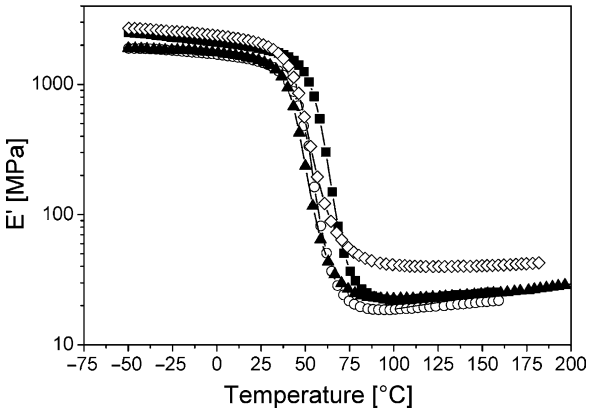

Fig. 7. Dynamic storage modulus E' at the frequency of 1 Hz, heating rate 3 °C/min. Silica content in phr: 0 (■), 10 (○), 20 (▲), 30 (◇).

silica particles on the fractured surface of 30 phr filled specimens.

Dynamic mechanical tensile tests at the frequency of 1 Hz were performed in order to measure the dynamic storage modulus (E') and the loss factor (tan δ) curves as a function of temperature. The storage modulus values were not constant in the glassy region but they slightly decreased with temperature (Fig. 7). As pointed out by Lewis and Nielsen [17], the residual stress field due to different thermal expansion coefficients of matrix and filler may induce relaxations in the polymeric phase accounting for the negative slope of E' versus temperature in the glassy region. Therefore, the representative values of the dynamic elastic modulus in the glassy region have been assessed by extrapolating the low temperature E' linear trend up to the peak temperature of the 1 Hz loss factor curve, assumed as T_g. The storage modulus values measured at 150 °C were arbitrarily considered as representative for the rubbery state, since for all samples a flat plateau above the glass transition temperature was not observed. In fact, except for the 30 phr filled samples, all the composites showed a positive slope in the graph of E' versus temperature. The values of dynamic storage moduli reported in Table 3 show a non-monotonic trend with the filler content as previously observed for tensile mechanical properties. The data also indicate that the reinforcing effect of the filler was higher in the rubbery state than in the glassy one. In Fig. 8 the experimental values of storage modulus E' are compared with theoretical predictions based on the Lewis–Nielsen [17,18] models (for the glassy and the rubbery states) and the Eiler–van Dick [19] models (for well dispersed and aggregated fillers). The samples filled with 10 and 20 phr silica clearly exhibited a reduction in tensile

Table 3
Dynamic storage modulus in the glassy and rubbery state

Silica content (phr)	E' glassy (MPa)	E' rubbery (MPa)
0	1410±160	25.0±1.0
10	1470±50	23.6±1.7
20	1380±130	29.7±4.0
30	1830±100	47.0±5.0

E' glassy, dynamic storage modulus linearly extrapolated to T_g; E' rubbery, dynamic storage modulus at 150 °C.

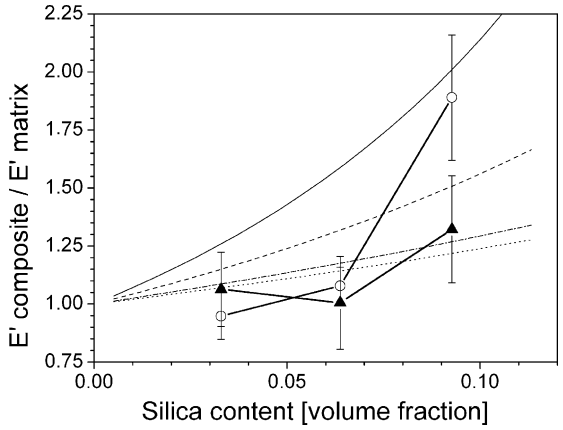

Fig. 8. Experimental values of relative storage modulus in the glassy (▲) and rubbery (○) state. Theoretical model, (EvD) Eiler–van Dick model for particulate filled composites in case of well dispersed (dashed line) and aggregated (solid line) filler; (LN) Lewis–Nielsen model for particulate filled polymeric matrix in the rubbery state (dash-dot line) and glassy state (dotted line).

modulus with respect to the unfilled matrix. These results can be explained on the basis of the reduction of the cross-linking degree of the matrix as observed in DSC scans. On the other hand at 30 phr filler level the composites behavior was in agreement with the theoretical prediction. Since for 30 phr filled samples DSC scans indicated a reduction in cross-linking degree of the polymeric matrix with respect to unfilled ones we still should expect poor mechanical performance by comparing the elastic modulus of the 30 phr filled composites with that of the unfilled, fully cross-linked matrix. The experimental results, on the contrary, suggested the occurrence of improved filler–matrix interactions in the 30 phr filled sample which seem to offset the reduced matrix stiffness due to incomplete cross-linking.

As reported in Fig. 9, the DMTA-loss factor curves of the composites were strongly affected by the filler content. The glass transition temperatures, measured as the loss factor peak at 1 Hz, are reported in Table 4. The data confirmed the trend observed in the DSC scans, with T_g's values decreasing and reaching a minimum for 20 phr silica and then increasing again for 30 phr silica. If the loss factor maxima are normalized by

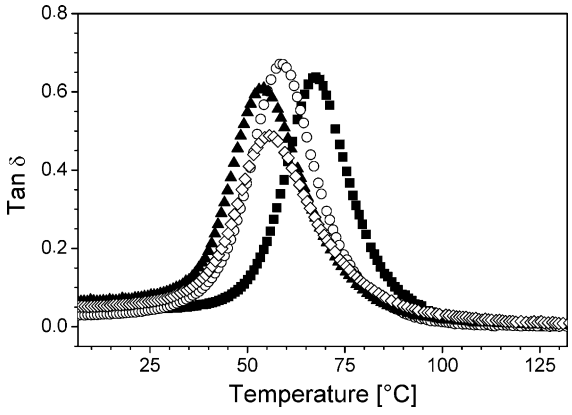

Fig. 9. Dynamic loss factor tan δ at the frequency of 1 Hz, heating rate 3 °C/min. Silica content in phr: 0 (■), 10 (○), 20 (▲), 30 (◇).

Table 4
Glass transition temperature and dynamic loss factor at the frequency of 1 Hz

Silica content (phr)	T_g (°C)	tan δ	tan δ^a
0	66.6±0.6	0.67±0.03	0.67±0.03
10	57.5±1.2	0.70±0.03	0.75±0.03
20	52.7±1.5	0.63±0.02	0.71±0.02
30	55.3±1.1	0.51±0.02	0.61±0.02

T_g, glass transition temperature as peak temperature of dynamic loss modulus at 1 Hz.
[a] Loss factor maxima normalized by the amount of polymeric matrix in the composites.

Table 5
Activation energy of molecular relaxation in the glassy and rubbery state

Silica content (phr)	E_a-glassy state (kJ/mol)	E_a-rubbery state (kJ/mol)	m at T_g (K)
0	60.8±0.4	174.6±0.2	20.2±0.8
10	56.7±0.8	162.7±0.1	18.6±0.4
20	72.2±0.7	156.6±1.0	17.3±0.1
30	81.2±0.6	161.1±0.8	18.9±0.6

E_a, activation energies calculated by fitting the linear portions of the shift factor curve with an Arrhenius type model; m at T_g, reticular cooperativity parameter calculated at the glass transition temperature.

the effective amount of polymeric phase in the system (see Table 4) an increase in the energy dissipation capacity can be observed in the nanocomposites filled with 10 and 20 phr silica, while samples filled with 30 phr silica show a reduction in the effective damping capacity.

These results are in agreement with the hypothesis of a reduction in the cross-link density of the epoxy matrix for 10 and 20 phr silica composites as previously reported for model epoxy resins with well defined network architecture [20,21]. The reduced damping capacity of 30 phr filled samples exhibited by the polymeric matrix suggests that the interaction with the filler may effectively lower the polymer mobility.

Multi-frequency DMTA tests provided the raw data required for the construction of the shift-factor curves according to the time–temperature superimposition principle (TTSP) as shown in Fig. 10. The shift factor $a_T^{T_g}$ for the equivalence between two isothermal curves of the storage modulus at T and T_g is defined as follows:

$$\log a_T^{T_g} = \log\left(\frac{f_{T_g}}{f}\right) \tag{1}$$

where T_g is the glass transition temperature assessed as the loss factor peak temperature at the frequency f_{T_g} of 1 Hz.

Both in the glassy and in the rubbery state, the obtained shift factor curves (see Fig. 10) are nearly linear on a logarithmic scale when plotted versus the reciprocal absolute temperature. A sigmoidal trend appears slightly before T_g. The activation energies for the molecular relaxation in the glassy and rubbery states were evaluated by fitting the linear portion of the shift factor curves with an Arrhenius type equation [22] in the following form:

$$\log a_T^{T_g} = \left(\frac{E_a}{R}\right)\left(\frac{1}{T} - \frac{1}{T_g}\right) \tag{2}$$

where E_a is the activation energy and R is the gas constant. The activation energies are summarized in Table 5. A reticular cooperativity parameter m was also calculated by taking the first derivative of the shift factor curve with respect to reciprocal absolute temperature as follows [23]:

$$m = \frac{\mathrm{d}(\log a_T^{T_g})}{\mathrm{d}(1/T)} \tag{3}$$

The reticular cooperativity parameter describes the homogeneity degree of the network architecture: the higher its value the more homogeneous is the structure and the narrower the statistical distribution of polymer segments between adjacent cross-link points. The values of the reticular cooperativity parameter are reported in Table 5 along with the activation energy in the rubbery state. It is worth noting that m was lower in the composites than in the unfilled samples thus confirming the hypothesis of the reduction in the cross-linking degree of the epoxy matrix due to the presence of silica particles. Both parameter E_a and m showed a minimum at 20 phr filler content and increased again for 30 phr filled samples being always lower than in the unfilled matrix. This trend closely resembled that one of the glass transition temperature. The values of the activation energies in the glassy state also exhibited a non-monotonic behavior but only in case

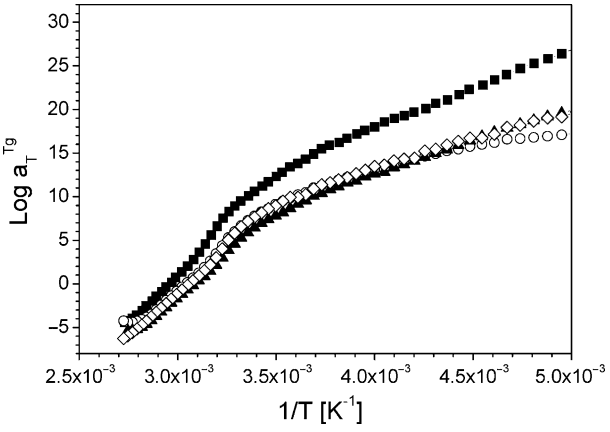

Fig. 10. Shift factor curves referred to the glass transition temperature of each sample. Silica content in phr: 0 (■), 10 (○), 20 (▲), 30 (◇).

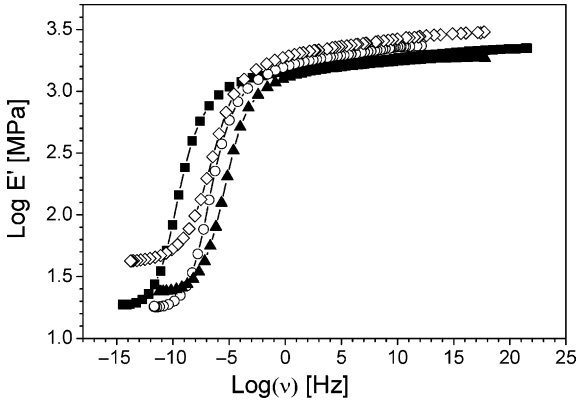

Fig. 11. Dynamic storage modulus master curve at the reference temperature of 25 °C. Silica content in phr: 0 (■), 10 (○), 20 (▲), 30 (◇).

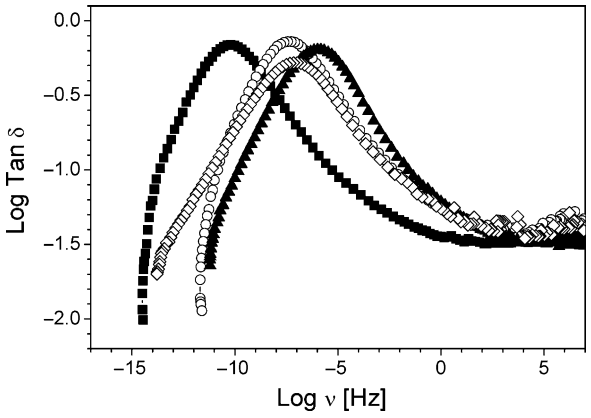

Fig. 12. Dynamic loss factor master curve at the reference temperature of 25 °C. Silica content in phr: 0 (■), 10 (○), 20 (▲), 30 (◇).

of 10 phr filled samples the activation energy was found to be lower than that of the unfilled matrix whereas it was remarkably higher for 20 and 30 phr filled samples. A possible explanation of these results should take into account that polymer–filler interactions may be more effective below the glass transition temperature since the existing secondary bonds (like H-bonds) are stronger than at higher temperatures.

The storage modulus and loss factor master curves are reported in Fig. 11 and in Fig. 12, respectively. The curves are arbitrarily referred to the temperature of 25 °C. The shapes of loss factor master curves for unfilled matrix, 10 and 20 phr filled samples are very similar being only shifted in the frequency domain as a result of the reduction of the glass transition temperature: the higher the T_g value the lower the frequency of the main spectral component in the relaxation spectrum. On the other hand, the loss factor master curve of 30 phr composites shows an evident broadening of the relaxation spectrum in the low frequency range corresponding to less mobile polymer chains. The presence of this spectral component could be interpreted as a proof of the existence of strong physical immobilization effects in 30 phr filled samples which were postulated to be responsible for offsetting the reduction in matrix cross-linking degree and determining the inversion observed in the thermo-mechanical properties.

4. Conclusions

The thermo-mechanical properties of the silica filled epoxy nanocomposites were found to decrease for 10 and 20 phr filled samples, while a trend inversion was observed for 30 phr filled samples.

The reduction of thermo-mechanical properties, such as glass transition temperatures, dynamic storage modulus and tensile modulus, was explained by postulating the presence of polymer–filler interactions limiting the cross-linking degree attained by the polymer matrix during composites curing. The inversion in properties trend at the highest filler content examined was supposed to be due to the enhanced physical immobilization effects experienced by the polymeric matrix near the percolation threshold of the filler. In fact, both SEM inspection of the fracture surfaces and dynamic mechanical multi-frequency tests suggested the existence of strong polymer–filler interactions in case of 30 phr filled samples. The results obtained and the abovementioned conclusions refer to the examined filler range and do not exclude the possibility that different effects could be observed at different filler content especially below the minimum examined value of 6.3% by weight.

The results obtained pointed out the key-role of matrix–filler interactions in determining the whole composite performances of the system analyzed and also suggested that their simple interpretation on the basis of the action of moisture residua cannot explain the complex non-monotonic behavior which were observed in the work.

Acknowledgements

This work was carried out with the financial support of the ‘Ministero dell’Istruzione dell’Università e della Ricerca’ (MIUR, Italy), PRIN 2003 (Grant No. 2003093440_002).

References

[1] Alexandre M, Dubois P. Mater Sci Eng 2000;28:1–63.
[2] Lan T, Pinnavaia TJ. Chem Mater 1994;6:2216–9.
[3] Pinnavaia TJ, Wang Z, Massam J. Polymer–clay nanocomposites. New York: Wiley; 2001 [chapter 7].
[4] Huang Y, Jiang S, Wu L, Hua Y. Polym Test 2004;23:9–15.
[5] Beloqui BJ, Fernandez-Gracia JC, Orgiles-Barcelo AC, Mahiques-Bugiada MM, Martin-Martinez JM. J Adhes Sci Technol 1999;13:695–711.
[6] Arrighi V, McEwen IJ, Quian H, Serraro Prieto MB. Polymer 2003;44:6259–66.
[7] Tsagaropoulos G, Eisemberg A. Macromolecules 1995;28:396–8.
[8] Tsagaropoulos G, Eisemberg A. Macromolecules 1995;28:6067–77.
[9] Sun Y, Zhang Z, Moon K, Wong CP. J Polym Sci: Part B 2004;42:3849–58.
[10] Cao YM, Sun J, Yu DH. J Appl Polym Sci 2002;83:70–7.
[11] Ash BJ, Schadler LS, Siegel RV. Mater Lett 2002;55:83–7.
[12] Xiong M, Gu G, You B, Wu L. J Appl Polym Sci 2003;90:1923–31.
[13] Kang S, Hong SI, Choe CR, Park M, Rim S, Kim J. Polymer 2001;42:879–87.
[14] Sun Y, Zhang Z, Moon K, Wong CP. J Polym Sci: Part B 2004;42:3849–58.
[15] Ellis TS, Karasz FE. Polymer 1984;25:665–9.
[16] Preghenella M, Pegoretti A, Migliaresi C. AFaM spectroscopy analysis of epoxy-silica nanocomposites. in preparation.
[17] Lewis TB, Nielsen LE. J Appl Polym Sci 1970;14:1449–71.
[18] Nielsen LE. J Compos Mater 1967;1:100–19.
[19] Ahmed S, Jones FR. J Mater Sci 1990;23:4933–42.
[20] Crawford E, Lesser AJ. J Polym Sci: Part B 1997;36:1371–82.
[21] Lesser AJ, Crawford E. J Appl Polym Sci 1997;66:387–95.
[22] Rongzhi L. Mater Sci Eng 2000;A278:36–45.
[23] Tyberg CS, Bergeron K, Sankarapandian M, Shih P, Loos AC, Dillard DA, et al. Polymer 2000;41:5053–62.